JOURNAL OF GEOPHYSICAL RESEARCH: SPACE PHYSICS, VOL. 118, 5454–5466, doi:10.1002/jgra.50519, 2013

Magnetospheric response to magnetosheath pressure pulses: A low-pass filter effect

M. O. Archer,[1] T. S. Horbury,[1] J. P. Eastwood,[1] J. M. Weygand,[2] and T. K. Yeoman[3]

Received 31 May 2013; revised 19 July 2013; accepted 15 August 2013; published 5 September 2013.

[1] We present observations from the magnetopause to the ground during periods of large amplitude, transient dynamic pressure pulses in the magnetosheath. While individual magnetosheath pulses are sharp and impulsive, the magnetospheric response is much smoother with frequencies in the Pc5–6 range being excited in the compressional and poloidal components of the magnetic field. We show that the magnetopause acts like a low-pass filter, suppressing timescales shorter than a few minutes. Further filtering appears to occur locally within the magnetosphere, which may be due to the unusual field line resonance frequency profile on this day. Ground magnetometer and radar data along with equivalent ionospheric currents show signatures of traveling convection vortices, similar to the response from pressure variations of solar wind origin. However, the signatures are associated with groups of magnetosheath pulses rather than individual ones due to the impulsive nature of the pressure variations. Thus, the scale-dependent magnetospheric response to these transient pressure variations results in coherent signatures on longer timescales than any individual pulse.

Citation: Archer, M. O., T. S. Horbury, J. P. Eastwood, J. M. Weygand, and T. K. Yeoman (2013), Magnetospheric response to magnetosheath pressure pulses: A low-pass filter effect, *J. Geophys. Res. Space Physics*, *118*, 5454–5466, doi:10.1002/jgra.50519.

1. Introduction

[2] Solar wind pressure variations can perturb the magnetopause, enhance the magnetospheric field, excite direct and resonant waves (often in the Pc5 range, i.e., 2–7 mHz) in the magnetosphere, and generate traveling convection vortices (TCVs) in the ionosphere [e.g., *Sibeck*, 1990, and references therein]. Pressure variations can also originate at the bow shock and ion foreshock, e.g., hot flow anomalies (HFAs) [e.g., *Burgess*, 1989; *Thomas et al.*, 1991], foreshock cavities [e.g., *Sibeck et al.*, 2002], and foreshock bubbles [*Omidi et al.*, 2010]. These transient phenomena are also known to have somewhat similar magnetospheric effects to those of solar wind origin [e.g., *Sibeck et al.*, 2003; *Hartinger et al.*, 2013]. In turn, Pc5 waves are believed to play a significant role in the mass, energy, and momentum transport within the Earth's magnetosphere: ULF waves accelerate auroral electrons [e.g., *Lotko et al.*, 1998] and are thought to play a role in mass transport [e.g., *Allan et al.*, 1986] and the energization and transport of radiation belt electrons [e.g., *Elkington et al.*, 1999].

[3] The position of the magnetopause in a steady state is given by a balance of the solar wind dynamic pressure and the magnetic pressure at the boundary. A number of approaches have been used to model perturbations about this equilibrium: *Smit* [1968] treated the nose of the magnetosphere as a rigid body, *Freeman et al.* [1995] considered the magnetopause analogous to an elastic membrane, and *Børve et al.* [2011] approximated the boundary as a perfectly conducting wall. All three models were linearized, resulting in damped harmonic oscillator equations of motion for the magnetopause driven by variations in the solar wind dynamic pressure. The calculated characteristic periods ranged from 2 to 12 min depending on solar wind conditions though were typically about 6 or 7 min, in agreement with observed magnetopause oscillations [e.g., *Anderson et al.*, 1968]. *Freeman et al.* [1995] and *Børve et al.* [2011] also predicted that the magnetopause motion would be strongly damped due to the relative motion of the magnetopause and solar wind, estimating the damping ratio (the level of damping relative to the critical case) to be $\sim$0.41. The theoretical transmissibility (ratio of output to input) of such a driven harmonic oscillator has a resonant peak of only 1.63: Much lower frequencies are fully transmitted whereas higher-frequency oscillations are increasingly suppressed. Therefore, the magnetopause is thought to act somewhat like a low-pass filter to pressure variations.

[4] Inside the magnetosphere, the local characteristic timescale is given by field line resonances (FLRs), standing Alfvén waves fixed at their ionospheric ends and usually

[1]Blackett Laboratory, Imperial College London, London, UK.
[2]Institute of Geophysics and Planetary Physics and Department of Earth and Space Sciences, University of California, Los Angeles, California, USA.
[3]Radio and Space Plasma Physics Group, Department of Physics and Astronomy, University of Leicester, Leicester, UK.

Corresponding author: M. O. Archer, Space and Atmospheric Physics Group, Blackett Laboratory, Imperial College London, Prince Consort Rd., London SW7 2BW, UK. (m.archer10@imperial.ac.uk)

2169-9380/13/10.1002/jgra.50519

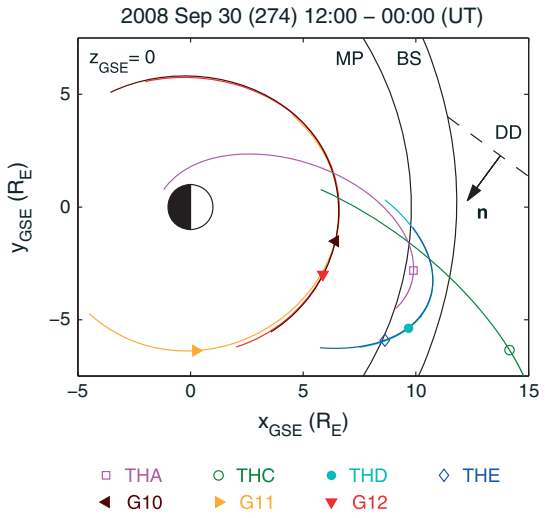

Figure 1. Orbits of the THEMIS and GOES spacecraft projected in the *x*-*y* GSE plane for 30 September 2008 12:00-00:00 UT. The spacecraft positions are shown for 15:00 UT. The magnetopause (MP) and bow shock (BS) are shown (solid lines) using the *Farris et al.* [1991] and *Peredo et al.* [1995] models, respectively. The estimated orientation of directional discontinuities (DD) in the solar wind on this day is indicated by the dashed line with corresponding normal **n**.

described in terms of poloidal and toroidal modes [e.g., *Southwood*, 1974]. Since the poloidal mode corresponds to radial motion of the plasma, implying the expansion and compression of the magnetosphere, it is necessarily coupled to the compressional mode via density fluctuations [*Kivelson et al.*, 1984]. However, mode conversion can also occur to the toroidal [e.g., *Warnecke et al.*, 1990]. *Gough and Orr* [1984] modeled these transverse mode oscillations again as a damped harmonic oscillator, driven by compressional waves due to magnetopause disturbances. By comparison with observations, they suggested that a damping ratio of 0.1 or greater is typical for the dayside magnetosphere. Whilst exhibiting a larger resonant peak, the suppression of higher frequencies is expected to be greater in this case than with the magnetopause models.

[5] Pressure variations in the magnetosheath can be used to test these models' predicted magnetospheric response. *Glassmeier et al.* [2008] showed that when the subsolar magnetosheath pressure varies on timescales of 5–7 min with amplitudes ∼0.5 nPa (∼50% the ambient value) the magnetopause motion and compression/expansion of the magnetospheric field are quasi-static. However, recently transient pulses in the magnetosheath dynamic pressure (sometimes called jets) have been reported [e.g., *Savin et al.*, 2008, 2011, 2012; *Hietala et al.*, 2009, 2012; *Amata et al.*, 2011]. These occur around 2% of the time, predominantly downstream of the quasi-parallel shock, and have durations of around 30 s on average and amplitudes of up to ∼15 times the ambient dynamic pressure (principally due to velocity increases) and ∼2 times the ambient total pressure [*Archer and Horbury*, 2013]. They also tend to be quasiperiodic, recurring on timescales of a few minutes (F. Plaschke et al., Anti-sunward high-speed jets in the subsolar magnetosheath, submitted to *Annales Geophysicae*, 2013).

[6] It is known that these pressure pulses or jets can have impacts within the magnetosphere. *Shue et al.* [2009] and *Amata et al.* [2011] showed that individual magnetosheath jets were able to distort and move the magnetopause ∼0.5–1.5 R_E. Irregular magnetic pulsations at geostationary orbit and localized flow enhancements in the ionosphere were reported by *Hietala et al.* [2012] to be caused by jets under steady quasi-radial interplanetary magnetic field (IMF). The "mesoscale" ionospheric signatures shared some similarities with magnetic impulse events (MIEs) and TCVs, though they did not appear to travel. In contrast, *Dmitriev and Suvorova* [2012] showed that a plasma jet due to a solar wind discontinuity resulted in a large-scale magnetopause distortion of an expansion-compression-expansion sequence lasting ∼15 min, effective penetration of magnetosheath plasma inside the magnetosphere, and traveling ground magnetometer signatures at low to middle latitudes over much larger spatial scales. It was unclear, however, how the discontinuity of duration ∼1 min resulted in a much longer timescale in the response.

[7] Whilst it is evident that magnetosheath pressure pulses can cause magnetopause motion, their subsequent effects and how these relate to other magnetospheric phenomena are not well understood. The response to quasiperiodic pulses, as opposed to isolated ones, is also unclear. In this paper we continue the study of *Archer et al.* [2012], who presented Time History of Events and Macroscale Interactions during Substorms (THEMIS) [*Angelopoulos*, 2008] observations of magnetosheath pressure pulses consistent with being generated by solar wind discontinuities interacting with the bow shock [*Lin et al.*, 1996a, 1996b; *Tsubouchi and Matsumoto*, 2005]. They showed evidence of magnetopause motion under the action of groups of pulses as opposed to isolated, individual ones. Here we use data from the THEMIS Fluxgate Magnetometer [*Auster et al.*, 2008] and Electrostatic Analyzer [*McFadden et al.*, 2008a], magnetometers from the GOES spacecraft [*Grubb*, 1975], ground magnetometers across North America and Greenland (THEMIS, Canadian Array for Realtime Investigations of Magnetic Activity (CARISMA), Canadian Magnetic Observatory System (CANMOS), Magnetometer Array for Cusp and Cleft Studies (MACCS), Geophysical Institute Magnetometer Array (GIMA), Technical University of Denmark (DTU), U.S. Geological Survey (USGS), and Solar-Terrestrial Energy Program (STEP)), and Super Dual Auroral Radar Network (SuperDARN) radar data [*Greenwald et al.*, 1995; *Chisham et al.*, 2007], which provide a comprehensive chain of observations from the magnetosheath to the ground in order to study the pulses' magnetospheric response.

2. Outer Magnetosphere

2.1. Observations

[8] Figure 1 shows the positions of the spacecraft on 30 September 2008. Between 15:01 UT and 22:47 UT, both THD and THE were in the magnetosheath, separated by ∼1 R_E and observed periods of large amplitude pressure pulses in the magnetosheath, shown in Figure 2 (first panel). The pressure pulses were typically of duration 10 s to 2 min in the spacecraft frame and tended to recur on timescales of 3–5 min; however, there were also large periods of time (of the order of an hour) when no pulses were observed at all.

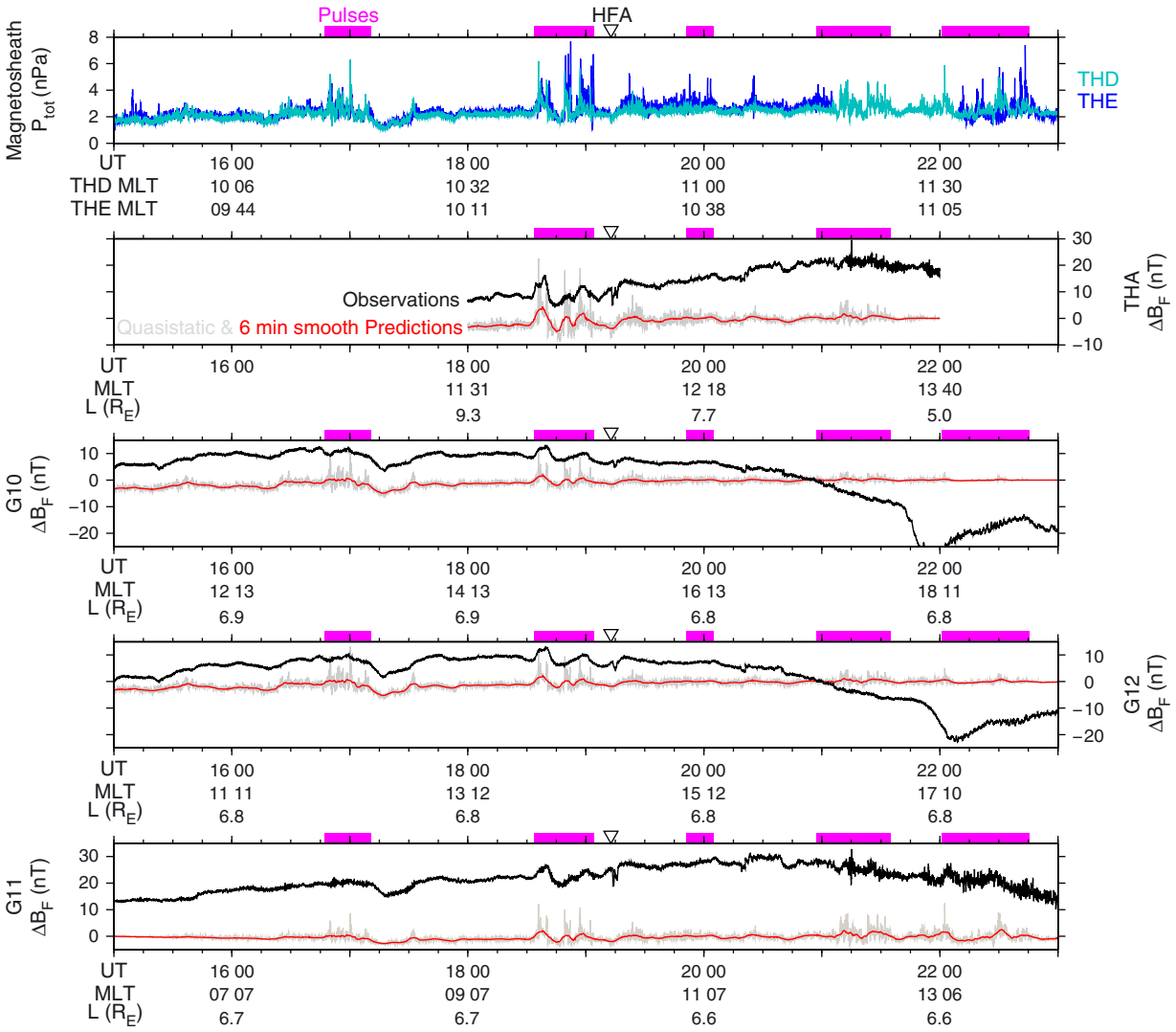

Figure 2. (first panel) Magnetosheath total pressure as measured by THD (turquoise) and THE (blue). Periods of pressure pulses are indicated by magenta bars and a pressure decrease consistent with a HFA is highlighted by the downward pointing triangle. (second to fifth panels) Changes in the mean field-aligned component of the magnetic field observed by THA and the three GOES spacecraft are given by the black lines where the predicted field magnitude from the T96 model for average upstream conditions has been subtracted. Predicted changes in field magnitude from T96 using THD observations are shown for quasi-static (grey) and 6 min smoothed (red) magnetospheric responses. Additional horizontal axes indicate the spacecraft magnetic local time (MLT) and L-shell.

The total pressure (ion thermal + electron thermal + dynamic + magnetic) of the pulses was 2–4 times that of the ambient plasma, with the enhancements chiefly being due to 3–10 times increases in the dynamic pressure. These dynamic pressure enhancements were mainly due to increases in the flow velocity [*Archer et al.*, 2012].

[9] Magnetic field data from THA and the GOES spacecraft were transformed into a mean field-aligned coordinate system (MFA) with the field-aligned component **F** (given by a 20 min moving average) representative of compressional modes, the azimuthal component $\mathbf{A} = \mathbf{F} \times \mathbf{r}$ (where **r** is the spacecraft's geocentric position, thus **A** points east) representative of toroidal Alfvénic modes, and the radial component **R** (completing the right-handed set pointing toward the Earth) representative of poloidal Alfvénic modes. Figure 2 shows the changes in the field-aligned component (black), where the predicted field magnitude from the T96 model [*Tsyganenko*, 1995; *Tsyganenko and Stern*, 1996] using average upstream conditions has been subtracted so that observed fluctuations are clearer. We only show THA data between 18:00 and 22:00 UT as a number of low-latitude boundary layer crossings were observed before then [*Archer et al.*, 2012] and afterward the magnetic field direction was changing faster than the averaging period, resulting in a poor estimate of **F**.

[10] Using the magnetosheath total pressure measurements as input to the T96 model, the predicted quasi-static response of the magnetosphere to pressure variations at the

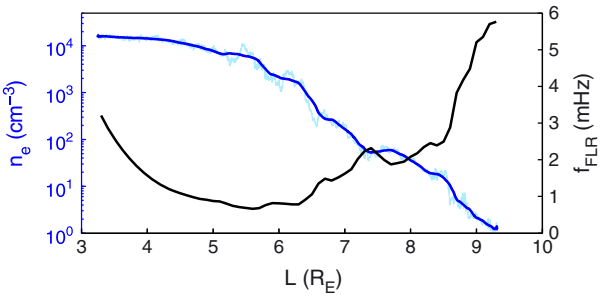

Figure 3. L-shell profiles of the magnetospheric electron number density observed by THA (light and dark blue, the latter has been smoothed) and the estimated fundamental field line resonant frequency (black).

spacecraft locations can be found as shown in Figure 2 (grey) using THD data. During intervals without pulses, the compressional variations of the magnetospheric field were similar to these predictions (with some systematic differences due to the statistical nature of the T96 model), consistent with *Glassmeier et al.* [2008]. It is clear, however, that the response to the pulses was different since the observed compressions of ∼1–10 nT (similar to those of *Hietala et al.* [2012] and *Dmitriev and Suvorova* [2012]) were much weaker and smoother than the sharp and impulsive magnetosheath pressure variations.

2.2. Analysis

[11] Although the magnetosheath pressure pulses contained variations over a wide range of frequencies due to their short timescales and quasiperiodicity, the harmonic oscillator models of the magnetopause [*Freeman et al.*, 1995; *Børve et al.*, 2011] predict a response somewhat like a low-pass filter with a typical timescale of about 6 or 7 min. Therefore, we smoothed the THD magnetosheath total pressure measurements by a 6 min running average (THE yielded qualitatively similar results) before inputting to the T96 model, giving more realistic predictions which are shown in Figure 2 (red). The predicted responses to the pulses, which could not be accounted for simply by the solar wind pressure, show good agreement with the magnetospheric observations overall. For the periods of pulses between 18:30 and 19:05 UT, the prediction yields three compressions of similar amplitude to those observed by THA and G11. THA also observed some higher frequencies which the smoothing does not capture, e.g., the two peaks in the 18:35 UT compression corresponding to two individual magnetosheath pressure pulses. These features were not as prominent at geostationary orbit, consistent with further filtering occurring at progressively lower L-shells. Between 21:00 and 23:00 UT, G11 and THA (when applicable) observations showed further agreement with the predictions (G10 and G12 were close to dusk during this period) though underestimated the response by ∼0.5–1 nT. Around 17:00 UT, the agreement was less clear, though both signatures were small at less than ∼0.5 nT.

[12] The predictions made through smoothing the magnetosheath pressure highlight the collective effect of pulses: The magnetospheric responses occurred over longer timescales and were due to many pulses rather than individual ones. This furthers the suggestion of *Hietala et al.* [2012] that pulses may have cumulative effects and that a one-to-one correspondence between individual pulses and their effects is not always clear. The filtering effect of the magnetopause may also account for the 15 min period response reported by *Dmitriev and Suvorova* [2012] due to a ∼1 min magnetosheath jet associated with a discontinuity, though the origin of the expansion-compression-expansion signature for that event is not clear since the magnetosheath pressure was only observed during the jet.

2.2.1. Time-Frequency Analysis

[13] Whilst a characteristic period of about 6 min is thought to be associated with the magnetopause, the local relevant timescale within the magnetosphere is that of field line resonances (FLRs) and these were estimated using the time of flight approximation:

$$f_{\mathrm{FLR}} = \left[2\int \frac{\mathrm{d}s}{v_A}\right]^{-1} \tag{1}$$

where f_{FLR} is the fundamental FLR frequency, v_A is the Alfvén speed, and the integration is carried out over the entire length of the field line. Note that we make no distinction between poloidal and toroidal mode FLRs in this calculation, though they are typically similar [*Cummings et al.*, 1969]. The average T96 model was used along with a power law density distribution along the field line [*Radoski and Carovillano*, 1966]:

$$\rho(L, r) = \rho_0(L)\left(\frac{L}{r}\right)^m \tag{2}$$

where r is the geocentric radial distance, L is the equatorial distance to the field line, $\rho_0(L)$ is the equatorial mass density, and the exponent m is taken to be 2 [*Denton et al.*, 2002; *Clausen et al.*, 2009]. Since THA traveled from the magnetopause to the inner magnetosphere close to the equatorial plane, $\rho_0(L)$ can be determined using equation (2) and the spacecraft potential inferred density [*McFadden et al.*, 2008b] shown in Figure 3. Unlike the standard magnetospheric density profile which shows a sharp jump in density at the plasmapause, the wave implications of which have been modeled extensively [e.g., *Lee and Lysak*, 1989], THA observed a steady increase in electron density of 4 orders of magnitude from $L \sim 9$–5 similar to that reported by *Tu et al.* [2007] during magnetospheric quiet times. In our calculation, the density was smoothed using a 20 min running average to remove fluctuations and the atomic mass was assumed to be 1. Assuming $\rho_0(L)$ did not change significantly over this interval, the FLR frequencies were also estimated for the GOES spacecraft. The calculations resulted in $f_{\mathrm{FLR}} \sim 0.5$–6 mHz, i.e., in the Pc5–6 range, though it should be noted that due to the density profile here, the configuration of the FLR frequencies is rather different to those previously modeled [e.g., *Lee and Lysak*, 1989]. Our computed frequencies are consistent with those obtained by *Wild et al.* [2005] using a similar method which were validated against numerical solutions to the wave equations as well as observed geomagnetic pulsations. While previous studies have shown that the difference between estimated FLR frequencies using different models can be large [*Berube et al.*, 2006; *McCollough et al.*, 2008], here it was found that using

a dipole model field changed the results by only ∼1 mHz at the largest L-shells and this difference rapidly became negligible with decreasing L-shell. Similarly, changing the exponent of the density distribution had little effect on the results. Thus, we are confident that our estimated frequencies are broadly correct; indeed in this study, we do not require precise FLR frequencies.

[14] To examine the frequency content of magnetospheric pulsations during intervals of magnetosheath pulses, dynamic spectra of the magnetic field data in the MFA system were calculated using the Morlet wavelet transform [*Torrence and Compo*, 1998]. The results for the field-aligned (with the mean field subtracted) and radial components are shown in Figure 4 for THA, G10, and G11 (G12 was similar to G10, an hour later in MLT) along with the phase difference when well defined (wavelet coherence [*Torrence and Webster*, 1999] greater than 0.75). The estimated first three harmonics of FLR frequencies are shown as the black lines. Also shown is the expected frequency of upstream ULF waves generated in the ion foreshock [*Takahashi et al.*, 1984] which are convected into the magnetosphere [e.g., *Clausen et al.*, 2009]:

$$f_{\mathrm{UW}}\,[\mathrm{mHz}] = 7.6B_0[\mathrm{nT}]\cos^2\theta_{Bx} \tag{3}$$

where B_0 is the IMF strength and θ_{Bx} is the IMF cone angle, calculated from 1 min smoothed (to remove contamination from upstream waves) THB data. At the spacecraft locations this was typically distinct from the FLR frequency. Pulsations at the upstream wave frequency are seen in Figure 4 often coincident with periods of pulses since they occur downstream of the quasi-parallel shock [*Archer et al.*, 2012].

[15] Figure 4 shows that THA observed, between 18:30 and 19:05 UT, large increases in the compressional mode power at the fundamental FLR frequency and below, with much less power at higher frequencies (apart from at the upstream wave frequency). The same interval observed by the GOES spacecraft, whilst lower power, also showed the largest increases at or below their respective fundamental FLR frequencies, which were lower than those for THA. Thus, further filtering of the compressional component occurred at lower L-shells. This may be due to the unusual FLR frequency profile on this day, which went down with decreasing L-shell from the magnetopause to $L \sim 6$. Near the magnetopause, broadband compressional waves at timescales of ∼3 min and longer would be expected due to the action of the pulses, as was observed by THA at around 18:35 UT. At each L-shell, compressional power may resonantly convert to toroidal modes, thus at a lower L-shell, there would appear to have been a filtering effect suppressing frequencies greater than the fundamental. It is beyond the scope of this study to discount other potential mechanisms of filtering under this unusual magnetospheric configuration. Future modeling and observational work could help distinguish between these mechanisms.

[16] During other periods of pulses, GOES observations again showed enhancements in the power typically at or below the FLR frequency. At around 21:00 UT, THA observed enhancements in power at frequencies ∼3 mHz which, while above the local FLR frequency, were consistent with the characteristic timescales of the magnetopause. Since we lack observations close to the magnetopause at this time, it is unclear whether this response is contrary to that reported for the earlier pulses or due to other effects.

[17] The dynamic spectra of the radial component of the magnetic field (indicating poloidal modes) were similar to the field-aligned component, but contained slightly less power. The coherence between the two components at Pc5–6 frequencies was generally good and the radial component lagged the field-aligned one, though the phase difference did not appear to be in perfect quadrature or even constant. The radial component of the magnetic field observed by THA between 18:30 and 19:05 UT was anticorrelated with the velocity fluctuations reported by *Archer et al.* [2012] (not shown here), consistent with poloidal Alfvén waves propagating parallel to the magnetic field.

[18] The azimuthal component of the magnetic field contained significantly less power with some evidence of toroidal mode FLRs (typically the first and second harmonics) due to magnetosheath pressure pulses with ∼0.2 nT amplitudes at geostationary orbit, comparable to those triggered by solar wind pressure pulses [*Sarris et al.*, 2010]. However, frequencies consistent with FLRs were also observed during some periods without any pulses. It should be noted that the magnetic perturbations associated with the fundamental toroidal mode are expected to be weak near the magnetic equator and thus difficult to observe by the spacecraft in this study [*Singer and Kivelson*, 1979]. Standing waves have a ±90° phase relationship between the electric and magnetic fields, however, testing this using wavelet analysis on data from THA's Electric Field Instrument [*Bonnell et al.*, 2008] proved inconclusive.

[19] On this day, there was a notable exception to the filtered magnetospheric response to pressure variations. A sharp drop in the magnetosheath pressure was observed by THC, THD, and THE at around 19:15 UT (indicated in figures by a triangle) due to a tangential discontinuity in the solar wind which satisfied the *Schwartz et al.* [2000] conditions for the formation of hot flow anomalies (HFAs). While no plasma data upstream of the shock were available, the magnetosheath observations were qualitatively similar to the HFA signatures reported by *Eastwood et al.* [2008] exhibiting flow deflections, magnetic field enhancements, density cavities, and hot plasma. The magnetospheric spacecraft observed a sharp decrease in the magnetic field due to the HFA (Figure 2) which consisted chiefly of frequencies at or above the fundamental FLR (Figure 4). Further work is required to understand why the magnetospheric response to HFAs is different to those expected purely from pressure variations.

2.2.2. Transfer Function

[20] We quantify the low-pass filter response of the magnetosphere by estimating the magnetopause pressure transfer function during periods of pressure pulses using data from THD and THA between 18:30 and 19:05 UT, since they were closest in MLT (just over an hour apart) and THA was only ∼1 R_E antisunward of the magnetopause. This gives an estimate of to what degree pressure balance at the magnetopause holds over different timescales. Using the wavelet transforms of the magnetosheath total pressure from THD and the magnetosphere magnetic pressure from THA, we calculate the ratio of the square-rooted time-averaged wavelet spectra over this interval (these are comparable

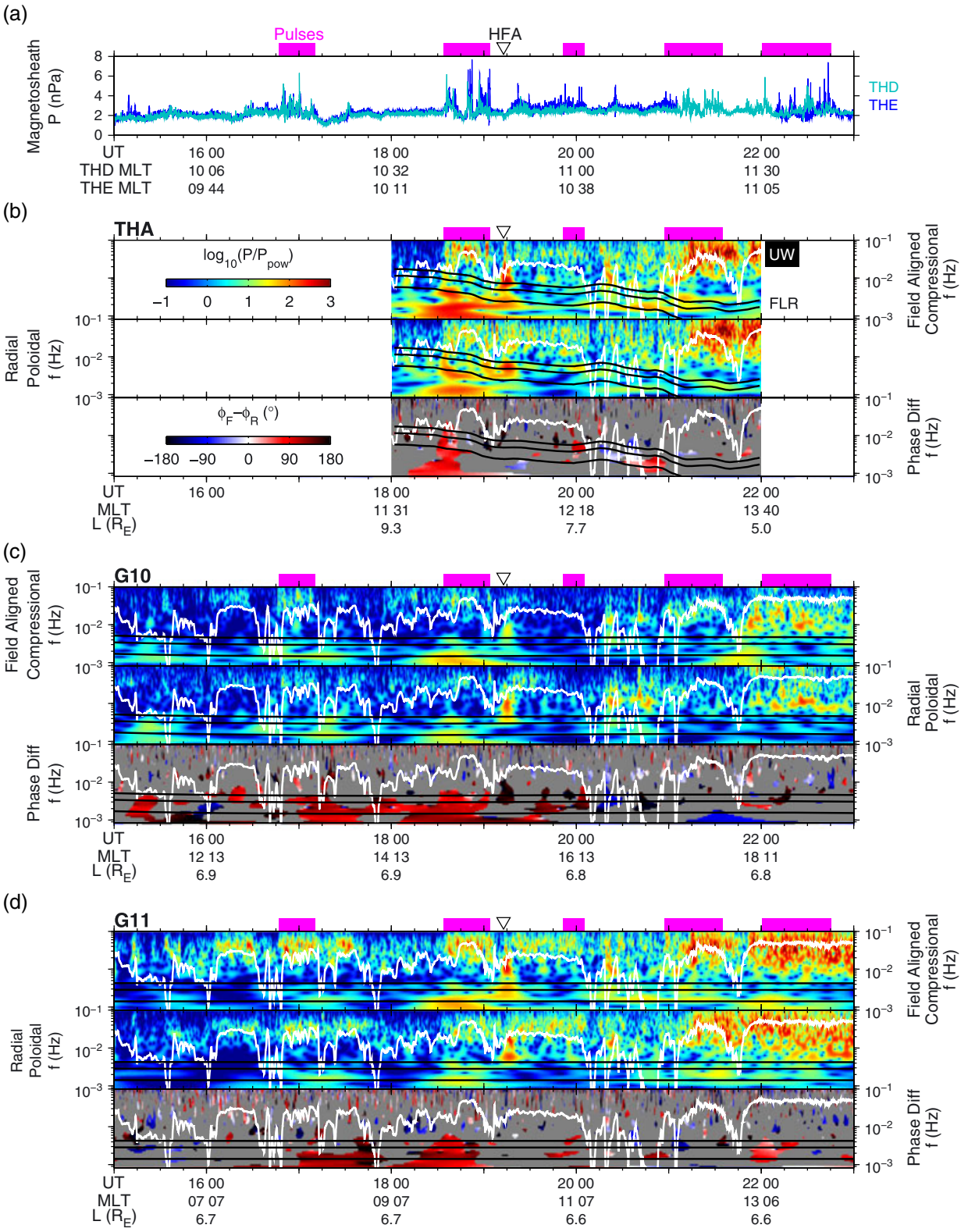

Figure 4. (a) Magnetosheath total pressure in the same format as Figure 2. (b-d) Dynamic power spectra from the wavelet transforms of the field-aligned and radial components of the magnetic field for THA, G10, and G11. The phase difference is also shown where grey areas indicate a wavelet coherence of less than 0.75. Estimates of the first three harmonics of field line resonances at the spacecrafts' location are indicated by the black lines. The expected frequency of upstream waves is shown as the white lines. Additional horizontal axes indicate the spacecraft magnetic local time (MLT) and L-shell.

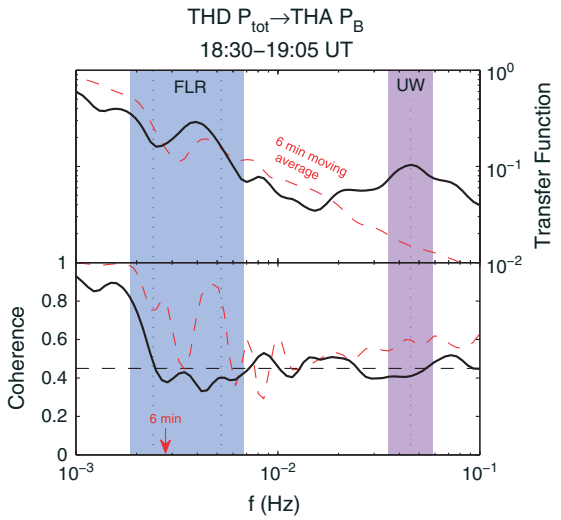

Figure 5. Estimate of the (top) magnetopause pressure transfer function and (bottom) corresponding coherence during the 18:30–19:05 UT magnetosheath pulses. The red dashed lines indicate the theoretical frequency response of a 6 min running average using the same method. Dotted blue lines indicate the range of field line resonant (FLR) frequencies over the interval used, with the light blue area also incorporating the spectral width of the Morlet wavelet. The magenta dotted line shows the average frequency of upstream waves (UW) during this interval, with the light purple area again indicating the width of the wavelet.

to Fourier power spectral densities [*Torrence and Compo*, 1998]). This transfer function is shown in Figure 5 (top) along with the corresponding time-averaged wavelet coherence (bottom), which can be interpreted as a local squared correlation coefficient at a given frequency.

[21] At frequencies below the local FLR frequency, the transfer function is large (∼0.5) and the coherence is close to unity at ∼0.9; hence, these frequencies are transmitted and the magnetopause reacts quasi-statically, consistent with *Glassmeier et al.* [2008]. At the lowest FLR frequency, the coherence drops to ∼0.45 varying by only ∼0.05, implying only some correlation between the magnetosheath and magnetosphere. The transfer function above the range of FLR frequencies, however, is small at ∼0.05. There is a small peak corresponding to the upstream wave frequency during this period; however, no increase in coherence is observed. Since upstream waves in the foreshock and magnetosphere are quasi-monochromatic [e.g., *Clausen et al.*, 2009] and magnetosheath pressure pulses are highly broadband, it is unlikely that the pulses are the mechanism by which foreshock ULF waves propagate through the magnetosheath. *Song et al.* [1993] suggested that the pressure variations associated with compressional waves in the magnetosheath cause the magnetopause to oscillate and reported that 17% of the Pc3–4 wave energy was transmitted across the magnetopause. The waves in their study had a frequency of ∼10 mHz, which according to our transfer function corresponds to ∼5% transmission. Since our magnetospheric observations are farther from the boundary (∼1 R_E), our results are not inconsistent with theirs.

[22] The red dashed lines in Figure 5 show the frequency response and coherence of a 6 min running average. These are somewhat similar to the observations with some notable differences: At frequencies above ∼20 mHz, the running average underestimates the transfer function and the peak in the coherence of the running average at ∼5 mHz is not observed. Therefore, whilst a 6 min running average does not precisely capture the response of the outer magnetosphere to the pressure variations, it nonetheless provides a reasonable first approximation.

3. Ground Magnetometers

3.1. Observations

[23] The times of the magnetosheath pressure pulses were such that many ground magnetometer (GMAG) stations across North America were on the dayside. Figure 6 displays examples from latitudinally separated (∼50° and 60° geomagnetic latitude) stations close to 12:00 MLT where the D (mean magnetic east) and H (mean magnetic north) components with the 2 h linear trend removed are shown (grey) along with 6 min smoothed data (black). Time lags (between ∼3 and 10 min) have been applied manually to the magnetosheath data to align with the GMAG data since accurately calculating such lags is difficult.

[24] Ionospheric Hall currents rotate magnetic pulsations by approximately 90° [*Hughes and Southwood*, 1976a, 1976b]; hence, the D component should chiefly contain poloidal mode waves, linked to the magnetospheric compressions. Indeed at The Pas (TPAS), B_D was very similar to the compressions observed by THA (compare with Figure 2). The lower latitude Pine Ridge (PINE) station observed smaller amplitudes and a much smoother response. This smoothing effect is similar to that noted when comparing THA observations to GOES. During the other periods of magnetosheath pressure pulses, there was some agreement with the variations in the D component and the smoothed magnetosheath pressure with some evidence of higher frequencies (other than the upstream wave frequency) being transmitted but suppressed, similar to the spacecraft observations. These features were observed by all dayside GMAGs, though the amplitude of the pulsations and their relative frequency content varied significantly between stations. Variations in the H component were unlike the D component, though they were found to resemble its negative time derivative, e.g., at 18:35 UT TPAS observed a positive excursion in the D component and a negative-positive bipolar signature in the H component. Such a relationship is often associated with traveling convection vortices [e.g., *Glassmeier et al.*, 1989].

3.2. Analysis

[25] To quantify the varying amplitudes of features and their relative timings, GMAG B_D observations were binned by magnetic longitude and the time intervals containing the response to groups of pulses were manually identified. The 2 h linear trend was removed from the time series and the time and amplitude of the largest peak within this interval was then found. The results for the group of pulses around 18:35 UT are shown in Figure 7 (those for around 18:50 UT proved similar), where the amplitudes are indicated by the size of the circles and their relative timings are

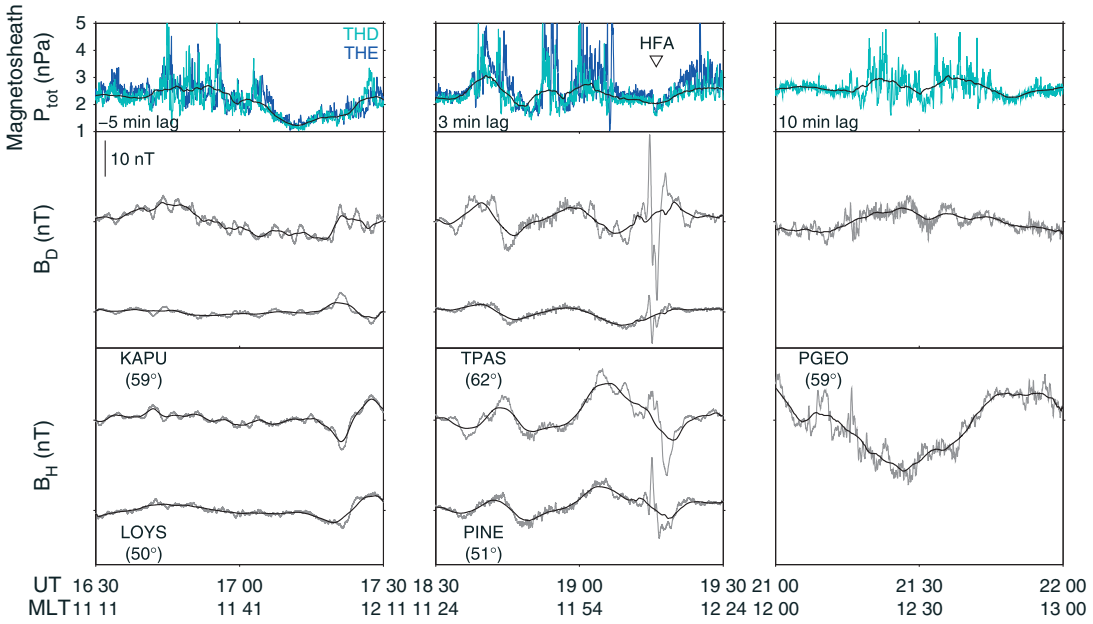

Figure 6. (top row) Magnetosheath total pressure as measured by THD (turquoise) and THE (blue). The black line shows the THD measurements smoothed by a 6 min running average. The applied time lags for the three panels are indicated and a HFA is highlighted by the downward pointing triangle. (middle and bottom rows) Stacked plots of GMAG data near the subsolar point. Grey lines show the detrended D and H components of the field, with 6 min smoothed data shown in black. Station names, geomagnetic latitudes, and the average magnetic local time are indicated also.

given by the colors. It is clear that the signatures tracked westward. We calculate the speed from a least squares linear fit of the high-latitude data to be 9 ± 2 km s^{-1}. Assuming events propagate through the ionosphere and magnetosphere with a constant angular velocity [*Korotova et al.*, 2002], this corresponds to a velocity of 245 ± 25 km s^{-1} at the magnetopause nose. The velocity along the normal of a rotational discontinuity is

$$v_n = \mathbf{v}_{sw} \cdot \mathbf{n} + v_A \quad (4)$$

where $\mathbf{v}_{sw}$ is the solar wind velocity vector, v_A is the Alfvén speed and the normal $\mathbf{n}$ (see Figure 1) was estimated by the cross-product method [e.g., *Knetter et al.*, 2004]. *Sibeck et al.* [2003] argue pressure variations approximately retain their solar wind alignment in the magnetosheath since the sum of the fast mode and convection velocities are of the order of the solar wind speed. Thus, we estimate the westward speed that the discontinuities associated with the group of pulses swept across the magnetopause to be 260 km s^{-1} (assuming a tangential discontinuity only

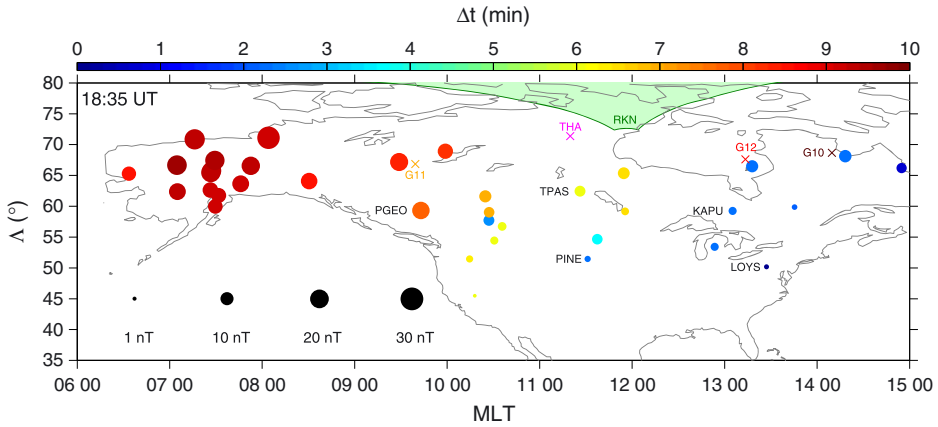

Figure 7. Map of North America in geomagnetic coordinates (magnetic local time along the horizontal and geomagnetic latitude Λ along the vertical) showing the response to the period of magnetosheath pulses at around 18:35 UT. GMAG stations are indicated by circles, where the amplitude of the observed pulsation in the D component is indicated by its size and their relative timings are given by the colors. The footprints (from the T96 model) of the spacecraft are shown as crosses and the field of view of the Rankin radars is given by the green area. The GMAG stations used in Figure 6 are also highlighted.

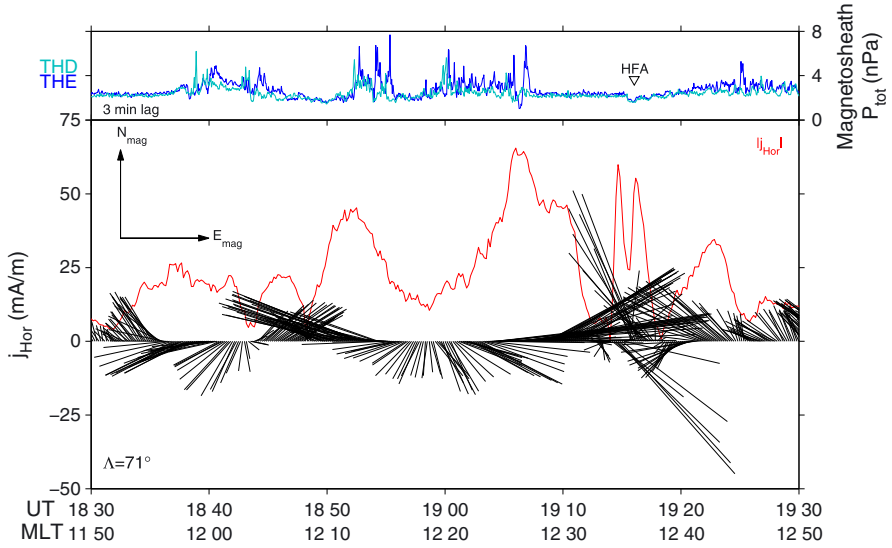

Figure 8. (top) Magnetosheath total pressure as measured by THD (turquoise) and THE (blue). (bottom) Feather plot of equivalent ionospheric currents at one grid point (with geomagnetic latitude 71° and the magnetic local time indicated in the horizontal axis) as a function of time, where geomagnetic north points upward and geomagnetic east to the right. The horizontal current magnitude is shown in red.

reduces this by ∼25 km s^{-1}), consistent with the estimate from the ground signatures. These results are comparable to *Dmitriev and Suvorova* [2012] who showed low- to middle-latitude GMAG signatures due to a single magnetosheath jet whose locations were consistent with the transition in shock geometries of a solar wind discontinuity and whose relative timings were in fair agreement with the discontinuity's motion.

[26] The amplitude of the ground signatures increased not only with magnetic latitude but also toward the west, e.g., at 65° geomagnetic latitude, it varied from ∼5 nT at 15:00 MLT to ∼30 nT at 07:30 MLT. This may be because the morning sector corresponded to a more quasi-parallel bow shock and thus perhaps larger pressure variations. Whilst such pulses are known to be most prevalent downstream of the quasi-parallel shock [*Archer and Horbury*, 2013], the factors that control their amplitude are unknown. Nonetheless, it is generally known that magnetopause motions and magnetic pulsations are greater prenoon rather than post-noon, corresponding to the location of the quasi-parallel bow shock under Parker spiral IMF [e.g., *Sibeck*, 1990]. There are of course many other factors which may affect the observed amplitudes on the ground including azimuthal wave number, frequency, density distribution along field lines, and ionospheric conductivity [e.g., *Sciffer and Waters*, 2011].

[27] Wavelet analysis was also performed on the D and H components of the GMAG data. The results were similar to the spacecraft data in Figure 4, with enhanced Pc5–6 frequencies during periods of magnetosheath pressure pulses. The peaks in the spectra during the pulses, while at different powers depending on latitude and MLT, were at the same frequencies for all stations; therefore, there was no evidence of L-shell-dependent FLRs observed on the ground.

4. Ionosphere

4.1. Equivalent Ionospheric Currents

[28] GMAG data can be used to calculate ionospheric currents using the spherical elementary current system method developed by *Amm and Viljanen* [1999]. *Weygand et al.* [2011] have applied this method to the GMAGs across North America and Greenland, finding that close to GMAG stations the derived currents were accurate to as good as 1% whereas in low coverage areas this was around 15%.

[29] An example time series of equivalent ionospheric currents (EICs), from the *Weygand et al.* [2011] database, during magnetosheath pressure pulses is shown in Figure 8, taken at 71° geomagnetic latitude and around 12:00 MLT between 18:30 and 19:30 UT. This grid point was only ∼310 km away from a GMAG station; therefore, the EICs are likely reliable. During the periods of magnetosheath pulses, there were enhancements in the horizontal currents (red). The directions of the currents showed two counterclockwise rotations between 18:30 and 19:10 UT. These signatures tracked westward like the magnetic deflections observed by the GMAGs. Assuming that ionospheric currents are composed mainly of Hall currents, EICs can be used as an approximation to the plasma convection. *Weygand et al.* [2012] showed that in general, the EICs derived from this method are antiparallel to the flows observed by the SuperDARN radars. Therefore, the counterclockwise rotations in Figure 8 are consistent with pairs of traveling convection vortices (TCVs), where the vortex centers were north of the grid point. Such pairs of vortices are expected from transient compressions of the magnetopause as they generate a pair of field-aligned currents which in turn have associated Hall current vortices [e.g., *Sibeck et al.*, 2003]. The timescales of these TCV signatures were close

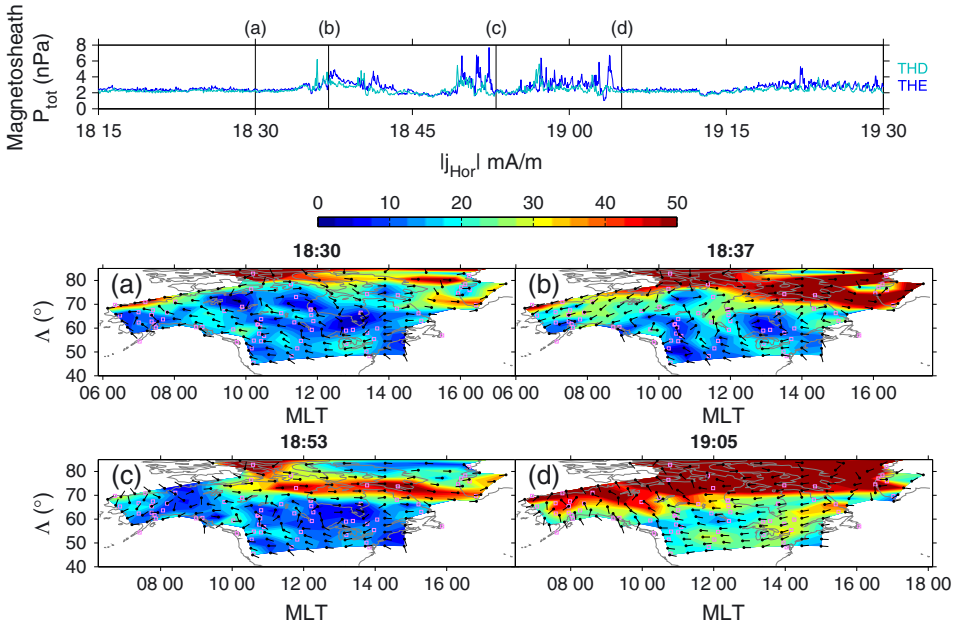

Figure 9. (top) Magnetosheath total pressure as measured by THD (turquoise) and THE (blue). Black vertical lines indicate the times corresponding to subsequent panels. (a–d) Maps of North America in geomagnetic coordinates (magnetic local time along the horizontal and geomagnetic latitude Λ along the vertical). The magnitude of equivalent ionospheric currents are given by the color scale and their direction are shown by the arrows. Magnetometer stations used in calculating the currents are indicated by pink squares.

to the peak of the distribution of TCVs by *Clauer and Petrov* [2002]. Current enhancements and signatures consistent with TCVs were again seen in the EICs between 21:00 and 22:00 UT (not shown) which corresponded to groups of magnetosheath pulses; however, this association was less clear at 17:00 UT due to a following decrease in the solar wind pressure.

[30] Figure 9 shows maps of the EICs, where Figure 9a is an example of the currents without magnetosheath pressure pulses and Figures 9b–9d show the responses to three groups of pulses. Contours of the current magnitude are shown as the colors whereas its direction is given by the arrows (which are generally smoothly varying suggesting they are reliable). The current was enhanced due to the groups of pulses most prominently at around 70° geomagnetic latitude and above (red areas in Figure 9). This is consistent with the occurrence distribution of magnetic impulse events (MIEs) often associated with TCVs [e.g., *Moretto et al.*, 2004]. Note that the number of magnetometers (pink squares) at these high latitudes is however small. The scale sizes of the current enhancements ranged from around 30° in magnetic longitude up to almost the entire dayside. It is helpful to convert timescales at the magnetopause into transverse scale sizes. Since we assume the discontinuities retain their solar wind alignment, the responses of ∼3–10 min in the outer magnetosphere correspond (through multiplying by the solar wind speed) to scale sizes along the Sun-Earth line of ∼13–42 R_E. Subsequently using the discontinuities' orientation yields transverse scale sizes at the magnetopause of ∼8–27 R_E, i.e.,∼30–160° magnetic longitude. Therefore, the scale sizes of the current enhancements are consistent with the timescales on which the magnetopause responds. The vortical structure associated with TCVs is not clear from the EIC maps, likely because the vortex centers were at higher latitudes than the locations of the majority of GMAG stations.

4.2. Radar Observations

[31] The Super Dual Auroral Radar Network (SuperDARN) uses radars to measure the line-of-sight component of the ionospheric **E**×**B** drift [*Greenwald et al.*, 1995] and on this day data were available from radars at Rankin and Inuvik. Figure 10 shows data from the Rankin radars (at around 10:15 MLT) in four beam directions between 16:15 and 17:15 UT (see Figure 7 for the field of view). Enhanced flows were observed in a number of beam directions and in at least one beam a reversal of line-of-sight velocity. The enhancements were typically strongest between 78 and 82° geomagnetic latitude, though coverage above this latitude was poor. Comparing these observations with the closest GMAGs showed them to correspond to the magnetic signatures of the pulses shown in Figure 6. The flow structures propagated westward (indicated by the arrow), seen from the relative timings at different beam directions (beam number increases toward east). Thus, SuperDARN observed a TCV (very similar to that reported by *Engebretson et al.* [2013]) due to a group of magnetosheath pressure pulses. While for other groups of pulses, further flow structures were observed, the data quality and coverage were often poor, and the azimuthal propagation between beam directions was not clear.

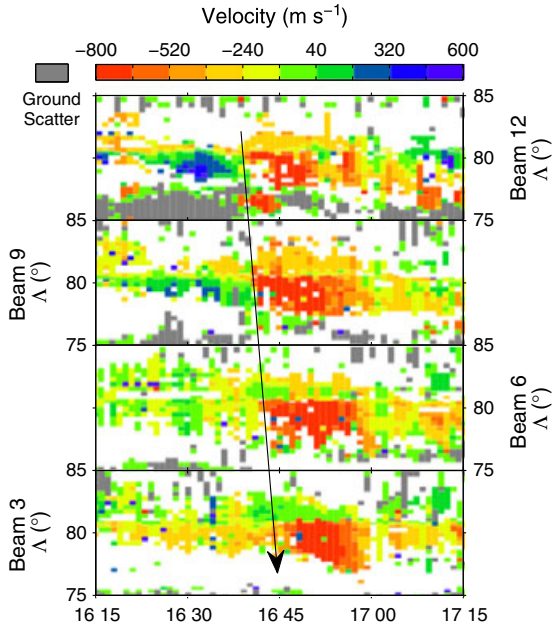

Figure 10. SuperDARN observations by the Rankin radars for a number of different beam directions. The color shows the ionospheric line-of-sight velocity at different geomagnetic latitudes Λ.

5. Discussion and Conclusions

[32] In this paper, the impact of large amplitude, transient dynamic pressure pulses in the magnetosheath has been investigated using observations from the magnetopause to the ground. The pulses triggered compressional and poloidal mode waves in the outer magnetosphere typically in the Pc5–6 range; such waves are important in the mass, energy, and momentum transport within Earth's magnetosphere [e.g., *Allan et al.*, 1986; *Lotko et al.*, 1998; *Elkington et al.*, 1999]. Solar wind pressure variations have similar effects [e.g., *Sibeck*, 1990], though these variations are generally on comparable timescales to their responses. In contrast, the magnetosheath pulses are sharp, impulsive, and quasiperiodic meaning they are much more broadband. Thus, the magnetopause and (under this unusual magnetospheric profile) lower L-shells process these variations resulting in much smoother responses with longer periods which are a collective effect of numerous pulses. This magnetospheric low-pass filter suppresses frequencies much higher than those characteristic to the magnetopause and local field line resonances, consistent with the suggestions of models [*Smit*, 1968; *Gough and Orr*, 1984; *Freeman et al.*, 1995; *Børve et al.*, 2011].

[33] The GMAG networks in North America allowed sampling over a large range of geomagnetic latitudes and magnetic local times. Signatures due to groups of pulses were observed in the D component, which traveled westward (i.e., tailward in the morning sector) at a speed in agreement with the solar wind discontinuities (associated with the pulses) sweeping across the magnetopause. The H component of the field varied like the negative time derivative of the D component, consistent with traveling convection vortices [e.g., *Glassmeier et al.*, 1989]. Equivalent ionospheric currents (EICs) also showed TCV signatures due to groups of pulses, assuming that the EICs consisted mostly of Hall currents. In addition, SuperDARN observations clearly showed TCV signatures due to one period of magnetosheath pulses. Therefore, the filtered response at the outer magnetosphere to a number of magnetosheath pressure pulses can collectively generate a pair of TCVs in the ionosphere. *Hietala et al.* [2012] presented SuperDARN data during an interval containing many magnetosheath jets, showing localized flow enhancements which were similar to TCVs but did not appear to travel. The differences between those observations and ours are likely due to the different mechanisms generating these pulses: They were not associated with solar wind discontinuities and the authors proposed the jets were due to ripples in the bow shock under steady quasi-radial IMF. This may explain their smaller scale sizes and why they did not travel tailward due to solar wind convection.

[34] *Archer and Horbury* [2013] showed that the majority of dynamic pressure enhancements in the magnetosheath were not associated with discontinuities in the solar wind and that the IMF was indeed steadier than usual during periods of pulses, suggesting that foreshock structures and processes are important in their generation. Recently, *Hartinger et al.* [2013] showed that transient ion foreshock phenomena can be a source of Pc5 waves in the magnetosphere. Since the response to the magnetosheath pressure pulses here was typically in the Pc5–6 range, this is suggestive that the signatures of transient ion foreshock phenomena in the magnetosheath may contain similar pressure pulses though further work is required.

[35] Finally, an interesting point is the difference in the magnetospheric response to the pressure pulses and the HFA. While models suggest that the magnetopause can only respond to pressure variations on timescales of the order of minutes or longer, consistent with the response to the pulses, the impact of the HFA was on much shorter timescales, though this was in agreement to previously reported events [e.g., *Eastwood et al.*, 2008; *Jacobsen et al.*, 2009]. The reason for the different temporal responses between the two transient phenomena could be addressed in the future.

[36] **Acknowledgments.** This research at Imperial College London was funded by STFC grant ST/I505713/1. J. P. Eastwood holds an STFC Advanced Fellowship at Imperial College London. The work of T. K. Yeoman was supported by STFC grant ST/H002480/1. We acknowledge NASA contract NAS5-02099 and V. Angelopoulos for use of data from the THEMIS Mission, specifically, C. W. Carlson and J. P. McFadden for use of ESA data; J. W. Bonnell and F. S. Mozer for use of EFI data; and K. H. Glassmeier, U. Auster and W. Baumjohann for the use of FGM data provided under the lead of the Technical University of Braunschweig and with financial support through the German Ministry for Economy and Technology and the German Center for Aviation and Space (DLR) under contract 50 OC 0302. For GOES magnetometer data, we thank H. J. Singer. For GMAG data, we thank S. Mende, C. T. Russell, I. R. Mann, D. K. Milling, M. Connors, E. Steinmetz, K. Hayashi, the CARISMA team, Tromsø Geophysical Observatory, Geophysical Institute University of Alaska, the Geological Survey of Canada, and the USGS Geomagnetism Program. The authors acknowledge the use of SuperDARN data. SuperDARN is a collection of radars funded by national scientific funding agencies of Australia, Canada, China, France, Japan, South Africa, United Kingdom, and United States of America. We also thank the reviewers for their comments.

[37] Masaki Fujimoto thanks Naiguo Lin and another reviewer for their assistance in evaluating this paper.

References

Allan, W., S. P. White, and E. M. Poulter (1986), Impulse-excited hydromagnetic cavity and field-line resonances in the magnetosphere, *Planet. Space Sci.*, *34*, 371–385, doi:10.1016/0032-0633(86)90144-3.

Amata, E., S. P. Savin, D. Ambrosino, Y. V. Bogdanova, M. F. Marcucci, S. Romanov, and A. Skalsky (2011), High kinetic energy density jets in the Earth's magnetosheath: A case study, *Planet. Space Sci.*, *59*, 482–494, doi:10.1016/j.pss.2010.07.021.

Amm, O., and A. Viljanen (1999), Ionospheric disturbance magnetic field continuation from the ground to the ionosphere using spherical elementary current systems, *Earth Planets Space*, *51*, 431–440.

Anderson, K. A., J. H. Binsack, and D. H. Fairfield (1968), Hydromagnetic disturbances of 3- to 15-minute period on the magnetopause and their relation to bow shock spikes, *J. Geophys. Res.*, *73*, 2371–2386, doi:10.1029/JA073i007p02371.

Angelopoulos, V. (2008), The THEMIS mission, *Space Sci. Rev.*, *141*, 5–34, doi:10.1007/s11214-008-9336-1.

Archer, M. O., and T. S. Horbury (2013), Magnetosheath dynamic pressure enhancements: Occurrence and typical properties, *Ann. Geophys.*, *31*, 319–331, doi:10.5194/angeo-31-319-2013.

Archer, M. O., T. S. Horbury, and J. P. Eastwood (2012), Magnetosheath pressure pulses: Generation downstream of the bow shock from solar wind discontinuities, *J. Geophys. Res.*, *117*, A05228, doi:10.1029/2011JA017468.

Auster, H. U., et al. (2008), The THEMIS fluxgate magnetometer, *Space Sci. Rev.*, *141*, 235–264, doi:10.1007/s11214-008-9365-9.

Berube, D., M. B. Moldwin, and M. Ahn (2006), Computing magnetospheric mass density from field line resonances in a realistic magnetic field geometry, *J. Geophys. Res.*, *111*, A08206, doi:10.1029/2005JA011450.

Bonnell, J. W., F. S. Mozer, G. T. Delory, A. J. Hull, R. E. Ergun, C. M. Cully, V. Angelopoulos, and P. R. Harvey (2008), The electric field instrument (EFI) for THEMIS, *Space Sci. Rev.*, *141*, 303–341, doi:10.1007/s11214-008-9469-2.

Børve, S., H. Sato, H. L. Pécseli, and J. K. Trulsen (2011), Minute-scale period oscillations of the magnetosphere, *Ann. Geophys.*, *29*, 663–671, doi:10.5194/angeo-29-663-2011.

Burgess, D. (1989), On the effect of a tangential discontinuity on ions specularly reflected at an oblique shock, *J. Geophys. Res.*, *94*, 472–478, doi:10.1029/JA094iA01p00472.

Chisham, G., et al. (2007), A decade of the Super Dual Auroral Radar Network (SuperDARN): Scientific achievements, new techniques and future directions, *Surv. Geophys.*, *28*, 33–109, doi:10.1007/s10712-007-9017-8.

Clauer, C. R., and V. G. Petrov (2002), A statistical investigation of traveling convection vortices observed by the west coast Greenland magnetometer chain, *J. Geophys. Res.*, *107*(A7), 1148, doi:10.1029/2001JA000228.

Clausen, L. B. N., T. K. Yeoman, R. C. Fear, R. Behlke, E. A. Lucek, and M. J. Engebretson (2009), First simultaneous measurements of waves generated at the bow shock in the solar wind, the magnetosphere and on the ground, *Ann. Geophys.*, *27*, 357–371, doi:10.5194/angeo-27-357-2009.

Cummings, W. D., R. J. O'Sullivan, and P. J. Coleman Jr. (1969), Standing Alfvén waves in the magnetosphere, *J. Geophys. Res.*, *74*, 778–793, doi:10.1029/JA074i003p00778.

Denton, R. E., J. Goldstein, J. D. Menietti, and S. L. Young (2002), Magnetospheric electron density model inferred from Polar plasma wave data, *J. Geophys. Res.*, *107*(A11), 1386, doi:10.1029/2001JA009136.

Dmitriev, A. V., and A. V. Suvorova (2012), Traveling magnetopause distortion related to a large-scale magnetosheath plasma jet: THEMIS and ground-based observations, *J. Geophys. Res.*, *117*, A08217, doi:10.1029/2011JA016861.

Eastwood, J. P., et al. (2008), THEMIS observations of a hot flow anomaly: Solar wind, magnetosheath, and ground-based measurements, *Geophys. Res. Lett.*, *35*, L17S03, doi:10.1029/2008GL033475.

Elkington, S. R., M. K. Hudson, and A. A. Chan (1999), Acceleration of relativistic electrons via drift-resonant interaction with toroidal-mode Pc5 ULF oscillations, *Geophys. Res. Lett.*, *26*, 3273, doi:10.1029/1999GL003659.

Engebretson, M. J., et al. (2013), Multi-instrument observations from Svalbard of a traveling convection vortex, electromagnetic ion cyclotron wave burst, and proton precipitation associated with a bow shock instability, *J. Geophys. Res. Space Physics*, *118*, 2975–2997, doi:10.1002/jgra.50291.

Farris, M. H., S. M. Petrinec, and C. T. Russell (1991), The thickness of the magnetosheath: Constraints on the polytropic index, *Geophys. Res. Lett.*, *18*, 1821–1824, doi:10.1029/91GL02090.

Freeman, M. P., N. C. Freeman, and C. J. Farrugia (1995), A linear perturbation analysis of magnetopause motion in the Newton-Busemann limit, *Ann. Geophys.*, *13*, 907–918, doi:10.1007/s00585-995-0907-0.

Glassmeier, K. H., M. Hönisch, and J. Untiedt (1989), Ground-based and satellite observations of traveling magnetospheric convection twin vortices, *J. Geophys. Res.*, *94*, 2520–2528, doi:10.1029/JA094iA03p02520.

Glassmeier, K.-H., et al. (2008), Magnetospheric quasi-static response to the dynamic magnetosheath: A THEMIS case study, *Geophys. Res. Lett.*, *35*, L17S01, doi:10.1029/2008GL033469.

Gough, H., and D. Orr (1984), The effect of damping on geomagnetic pulsation amplitude and phase at ground observatories, *Planet. Space Sci.*, *32*, 619–628, doi:10.1016/0032-0633(84)90112-0.

Greenwald, R. A., et al. (1995), DARN/SuperDARN: A global view of the dynamics of high-latitude convection, *Space Sci. Rev.*, *71*, 761–796.

Grubb, R. N. (1975), The SMS/GOES space environment monitor subsystem, NOAA technical memorandum ERL SEL 42., National Oceanic and Atmospheric Administration.

Hartinger, M. D., D. L. Turner, F. Plaschke, V. Angelopoulos, and H. Singer (2013), The role of transient ion foreshock phenomena in driving Pc5 ULF wave activity, *J. Geophys. Res. Space Physics*, *118*, 299–312, doi:10.1029/2012JA018349.

Hietala, H., et al. (2009), Supermagnetosonic jets behind a collisionless quasiparallel shock, *Phys. Rev. Lett.*, *103*, 245,001, doi:10.1103/PhysRevLett.103.245001.

Hietala, H., et al. (2012), Supermagnetosonic subsolar magnetosheath jets and their effects: From the solar wind to the ionospheric convection, *Ann. Geophys.*, *30*, 33–48, doi:10.5194/angeo-30-33-2012.

Hughes, W. J., and D. J. Southwood (1976a), The screening of micropulsation signals by the atmosphere and ionosphere, *J. Geophys. Res.*, *81*, 3234–3240, doi:10.1029/JA081i019p03234.

Hughes, W. J., and D. J. Southwood (1976b), An illustration of modification of geomagnetic pulsation structure by the ionosphere, *J. Geophys. Res.*, *81*, 3241–3247, doi:10.1029/JA081i019p03234.

Jacobsen, K. S., et al. (2009), THEMIS observations of extreme magnetopause motion caused by a hot flow anomaly, *J. Geophys. Res.*, *114*, A08210, doi:10.1029/2008JA013873.

Kivelson, M., J. Etcheto, and J. G. Trotignon (1984), Global compressional oscillations of the terrestrial magnetosphere: The evidence and a model, *J. Geophys. Res.*, *89*, 9851–9856, doi:10.1029/JA089iA11p09851.

Knetter, T., F. M. Neubauer, T. Horbury, and A. Balogh (2004), Four-point discontinuity observations using Cluster magnetic field data: A statistical survey, *J. Geophys. Res.*, *109*, A06102, doi:10.1029/2003JA010099.

Korotova, G. I., D. G. Sibeck, H. J. Singer, and T. J. Rosenberg (2002), Tracking transient events through geosynchronous orbit and in the high-latitude ionosphere, *J. Geophys. Res.*, *107*(A11), 1345, doi:10.1029/2002JA009477.

Lee, D.-H., and R. L. Lysak (1989), Magnetospheric ULF wave coupling in the dipole model: The impulsive excitation, *J. Geophys. Res.*, *94*, 17,097–17,103, doi:10.1029/JA094iA12p17097.

Lin, Y., L. C. Lee, and M. Yan (1996a), Generation of dynamic pressure pulses downstream of the bow shock by variations in the interplanetary magnetic field orientation, *J. Geophys. Res.*, *101*, 479–493, doi:10.1029/95JA02985.

Lin, Y., D. W. Swift, and L. C. Lee (1996b), Simulation of pressure pulses in the bow shock and magnetosheath driven by variations in interplanetary magnetic field direction, *J. Geophys. Res.*, *101*, 27,251–27,269, doi:10.1029/96JA02733.

Lotko, W., A. V. Streltsov, and C. W. Carlson (1998), Discrete auroral arc, electrostatic shock and suprathermal electrons powered by dispersive, anomalously resistive field line resonance, *Geophys. Res. Lett.*, *25*, 4449–4452, doi:10.1029/1998GL900200.

McCollough, J. P., J. L. Gannon, D. N. Baker, and M. Gehmeyr (2008), A statistical comparison of commonly used external magnetic field models, *Space Weather*, *6*, S10001, doi:10.1029/2008SW000391.

McFadden, J. P., C. W. Carlson, D. Larson, M. Ludlam, R. Abiad, B. Elliott, P. Turin, M. Marckwordt, and V. Angelopoulos (2008a), The THEMIS ESA plasma instrument and in-flight calibration, *Space Sci. Rev.*, *141*, 277–302, doi:10.1007/s11214-008-9440-2.

McFadden, J. P., C. W. Carlson, J. Bonnell, F. Mozer, V. Angelopoulos, K. H. Glassmeier, and U. Auster (2008b), THEMIS ESA first science results and performance issues, *Space Sci. Rev.*, *141*, 447–508, doi:10.1007/s11214-008-9433-1.

Moretto, T., D. Sibeck, and J. F. Watermann (2004), Occurrence statistics of magnetic impulse events, *Ann. Geophys.*, *22*, 585–602, doi:10.5194/angeo-22-585-2004.

Omidi, N., J. P. Eastwood, and D. G. Sibeck (2010), Foreshock bubbles and their global magnetospheric impacts, *J. Geophys. Res.*, *115*, A06204, doi:10.1029/2009JA014828.

Peredo, M., J. A. Slavin, E. Mazur, and S. A. Curtis (1995), Three-dimensional position and shape of the bow shock and their variation with Alfvénic, sonic and magnetosonic Mach numbers and interplanetary magnetic field orientation, *J. Geophys. Res.*, *100*, 7907–7916, doi:10.1029/94JA02545.

Radoski, H. R., and R. L. Carovillano (1966), Axisymmetric plasmasphere resonances: Toroidal mode, *Phys. Fluids*, *9*, 285, doi:10.1063/1.1761671.

Sarris, T. E., W. Liu, X. Li, K. Kabin, E. R. Talaat, R. Rankin, V. Angelopoulos, J. Bonnell, and K. H. Glassmeier (2010), THEMIS observations of the spatial extent and pressure-pulse excitation of field line resonances, *Geophys. Res. Lett.*, *37*, L15104, doi:10.1029/2010GL044125.

Savin, S., et al. (2008), High energy jets in the Earth's magnetosheath: Implications for plasma dynamics and anomalous transport, *JETP Lett.*, *87*, 593–599, doi:10.1134/S0021364008110015.

Savin, S., et al. (2011), Anomalous interaction of a plasma flow with the boundary layers of a geomagnetic trap, *JETP Lett.*, *93*, 754–762, doi:10.1134/S0021364011120137.

Savin, S., et al. (2012), Super fast plasma streams as drivers of transient and anomalous magnetospheric dynamics, *Ann. Geophys.*, *30*, 1–7, doi:10.5194/angeo-30-1-2012.

Schwartz, S. J., G. Paschmann, N. Sckopke, T. M. Bauer, M. Dunlop, A. N. Fazakerley, and M. F. Thomsen (2000), Conditions for the formation of hot flow anomalies at Earth's bow shock, *J. Geophys. Res.*, *105*, 12,639–12,650, doi:10.1029/1999JA000320.

Sciffer, M. D., and C. L. Waters (2011), Relationship between ULF wave mode mix, equatorial electric fields, and ground magnetometer data, *J. Geophys. Res.*, *116*, A06202, doi:10.1029/2010JA016307.

Shue, J.-H., J.-K. Chao, P. Song, J. P. McFadden, A. Suvorova, V. Angelopoulos, K. H. Glassmeier, and F. Plaschke (2009), Anomalous magnetosheath flows and distorted subsolar magnetopause for radial interplanetary magnetic fields, *Geophys. Res. Lett.*, *36*, L18112, doi:10.1029/2009GL039842.

Sibeck, D. G. (1990), A model for the transient magnetospheric response to sudden solar wind dynamic pressure variations, *J. Geophys. Res.*, *95*, 3755–3771, doi:10.1029/JA095iA04p03755.

Sibeck, D. G., T.-D. Phan, R. Lin, R. P. Lepping, and A. Szabo (2002), Wind observations of foreshock cavities: A case study, *J. Geophys. Res.*, *107*(A10), 1271, doi:10.1029/2001JA007539.

Sibeck, D. G., N. B. Trivedi, E. Zesta, R. B. Decker, H. J. Singer, A. Szabo, H. Tachihara, and J. Watermann (2003), Pressure-pulse interaction with the magnetosphere and ionosphere, *J. Geophys. Res.*, *108*(A2), 1095, doi:10.1029/2002JA009675.

Singer, H. J., and M. G. Kivelson (1979), The latitudinal structure of Pc 5 waves in space: Magnetic and electric field observations, *J. Geophys. Res.*, *84*, 7213–7222, doi:10.1029/JA084iA12p07213.

Smit, G. R. (1968), Oscillatory motion of the nose region of the magnetopause, *J. Geophys. Res.*, *73*, 4990–4993, doi:10.1029/JA073i015p04990.

Song, P., C. T. Russell, R. J. Strangeway, J. R. Wygant, C. A. Cattell, R. J. Fitzenreiter, and R. R. Anderson (1993), Wave properties near the subsolar magnetopause: Pc3–4 energy coupling for northward interplanetary magnetic field, *J. Geophys. Res.*, *98*, 187–196, doi:10.1029/92JA01534.

Southwood, D. J. (1974), Some features of field line resonances in the magnetosphere, *Planet. Space Sci.*, *22*, 483–491, doi:10.1016/0032-0633(74)90078-6.

Takahashi, K., R. L. McPherron, and T. Terasawa (1984), Dependence of the spectrum of Pc3–4 pulsations on the interplanetary magnetic field, *J. Geophys. Res.*, *89*, 2770–2780, doi:10.1029/JA089iA05p02770.

Thomas, V. A., D. Winske, M. F. Thomsen, and T. G. Onsager (1991), Hybrid simulation of the formation of a hot flow anomaly, *J. Geophys. Res.*, *96*, 11,625–11,632, doi:10.1029/91JA01092.

Torrence, C., and G. P. Compo (1998), A practical guide to wavelet analysis, *Bull. Am. Meteorol. Soc.*, *79*, 61–78, doi:10.1175/1520-0477(1998)079<0061:APGTWA>2.0.CO;2.

Torrence, C., and P. Webster (1999), Interdecadal changes in the ENSO–Monsoon system, *J. Clim.*, *12*, 2679–2690, doi:10.1175/1520-0442(1999)012<2679:ICITEM>2.0.CO;2.

Tsubouchi, K., and H. Matsumoto (2005), Effect of upstream rotational field on the formation of magnetic depressions in a quasi-perpendicular shock downstream, *J. Geophys. Res.*, *110*, A04101, doi:10.1029/2004JA010818.

Tsyganenko, N. A. (1995), Modeling the Earth's magnetospheric magnetic field confined within a realistic magnetopause, *J. Geophys. Res.*, *100*, 5599–5612, doi:10.1029/94JA03193.

Tsyganenko, N. A., and D. P. Stern (1996), Modeling the global magnetic field of the large-scale Birkeland current systems, *J. Geophys. Res.*, *101*, 27,187–27,198, doi:10.1029/96JA02735.

Tu, J., P. Song, B. W. Reinisch, and J. L. Green (2007), Smooth electron density transition from plasmasphere to the subauroral region, *J. Geophys. Res.*, *112*, A05227, doi:10.1029/2007JA012298.

Warnecke, J., H. Lühr, and K. Takahashi (1990), Observational features of field line resonances excited by solar wind pressure variations on 4 September 1984, *Planet. Space Sci.*, *38*, 1517–1531, doi:10.1016/0032-0633(90)90157-L.

Weygand, J. M., O. Amm, A. Viljanen, V. Angelopoulos, D. Murr, M. J. Engebretson, H. Gleisner, and I. Mann (2011), Application and validation of the spherical elementary currents systems technique for deriving ionospheric equivalent currents with the North American and Greenland ground magnetometer arrays, *J. Geophys. Res.*, *116*, A03305, doi:10.1029/2010JA016177.

Weygand, J. M., O. Amm, V. Angelopoulos, S. E. Milan, A. Grocott, H. Gleisner, and C. Stolle (2012), Comparison between SuperDARN flow vectors and equivalent ionospheric currents from ground magnetometer arrays, *J. Geophys. Res.*, *117*, A05325, doi:10.1029/2011JA017407.

Wild, J. A., T. K. Yeoman, and C. L. Waters (2005), Revised time of flight calculations for high latitude geomagnetic pulsations using a realistic magnetospheric magnetic field model, *J. Geophys. Res.*, *110*, A11206, doi:10.1029/2004JA010964.